JOURNAL OF MATERIALS SCIENCE 27 (1992) 5939–5947

Tensile behaviour of Ni_3Al+B intermetallic compound: influence of cold deformation and annealing

T. S. SRIVATSAN, S. ANAND, S. SRIRAM*
Department of Mechanical Engineering, The University of Akron, Akron, OH 44325, USA
T. S. SUDARSHAN
Materials Modification Inc., PO Box 4817, Falls Church, VA 22044, USA

Nickel aluminide, intermetallic compound Ni_3Al, is a promising structural material on account of its high strength at elevated temperatures. The influence of cold deformation on the tensile behaviour of an Ni_3Al alloy containing zirconium and boron is presented. The undeformed material, in the as-cast condition, was subjected to varying levels of cold deformation ranging from 11.4%–61.4%, and tensile tests performed. The tensile properties and fracture behaviour of the cold-deformed material are compared with undeformed material to highlight the influence of cold deformation on strength, ductility and fracture behaviour. Tensile tests were performed on cold-deformed plus annealed samples and properties compared with the cold-deformed counterpart in order to elucidate the influence of annealing on tensile behaviour. The intrinsic effects of cold deformation and annealing on microstructure, tensile properties and fracture behaviour are highlighted.

1. Introduction

Rapid advances in aerospace technology have created a need for a new generation of structural materials. Ordered intermetallic compounds constitute a unique class of metallic materials which have shown promise for replacing conventional nickel-based superalloys. These compounds have been recognized for their superior strength coupled with superior resistance to creep, fatigue and corrosion resistance at elevated temperatures. The tendency for chemical ordering in these intermetallic compounds reduces atom mobility at elevated temperatures resulting in good structural stability and resistance to high-temperature deformation [1]. The NiAl and Ni_3Al ordered intermetallic compounds of nickel and aluminium have, in recent years, been the subject of increasing research activity because of their excellent oxidation resistance, fairly high melting temperatures and relatively low densities which make them particularly attractive for potential use as aircraft engine materials.

The Ni_3Al intermetallic compound is of interest for use at elevated temperatures, primarily because its yield strength actually increases rather than decreases with an increase in temperature [2–4]. However, use of these nickel aluminides, in polycrystalline form, as an engineering material is rendered difficult on account of their low ductility and poor fracture-related properties at ambient temperature [5–9]. The low ductility and tendency for brittle intergranular fracture was a major obstacle that limited the development of polycrystalline Ni_3Al alloys as engineering materials. The inferior ductility of the intermetallic compound was attributed to concurrent and competing influences of [10–15]:

(a) a low cohesive strength of grain boundaries;

(b) embrittling effects of impurities at the grain boundaries;

(c) a tendency to fail by brittle intergranular fracture mode; and

(d) a low initial density of mobile dislocations.

In general, techniques for improving the low ductility, inadequate fracture toughness and poor fracture-related properties of the ordered intermetallic compound, Ni_3Al, fall into two broad categories:

(i) microstructural modifications through a refinement in grain size and ensuing difficulty in grain boundary crack initiation and propagation,

(ii) compositional modifications through methods of enhancing the probability of (1 1 1) slip by lowering the antiphase energy and/or improving the cohesive strength of grain boundaries. This also facilitates enhancing the ductility of polycrystalline Ni_3Al specifically at cryogenic temperatures.

The segregation of impurities to grain boundaries weakens them and promotes premature fracture before macroscopic yield can occur. However, recent

* *Present address*: A. C. T. Consulting Inc., Canton, OH 44718, USA.

0022–2461

studies have convincingly shown that the fracture toughness of Ni_3Al is good, despite the grain boundary being intrinsically brittle [16, 17].

In recent years, alloy design efforts have focused on compositional modifications as a means of improving the room-temperature ductility and fracture-related properties of Ni_3Al-based alloys. The effects of small addition of boron to Ni_3Al have been studied by several groups of investigators [13–26]. Small additions of boron substantially eliminated the intergranular brittleness problem associated with pure Ni_3Al [13, 18, 20]. Interest in the use of boron as a microalloying addition was triggered by an elimination of the intergranular brittleness with a concomitant improvement in the room-temperature ductility of the polycrystalline Ni_3Al alloy due to a change in fracture mode from brittle intergranular to predominantly ductile transgranular fracture in smooth tensile specimens. The change in macroscopic fracture mode was attributed to boron enrichment at grain boundaries as revealed by Auger spectroscopy [13, 23, 24]. The improvement in ductility and fracture properties opened the possibility of practical applications for this novel engineering material.

There are two hypotheses explaining the phenomenon of ductility improvement [13, 27–29]. The first one [13, 27] is based on an assumption that boron segregation to grain boundaries in Ni_3Al leads to an increase of cohesive strength across the grain boundary, due to the formation of strong interatomic bonds according to the theory of Briant and Messmer [30, 31]. The increased grain-boundary strength enables higher levels of stress to be applied to a polycrystalline specimen, thereby, activating slip before reaching the grain-boundary fracture strength. White *et al.* [27] attributed the improvement in ductility of Ni_3Al resulting from boron addition to an actual improvement in grain-boundary cohesive strength.

The other hypotheses [28, 29] assumes that reduced ordering of grain-boundary regions due to boron segregation leads to an increased mobility of grain-boundary dislocations. Owing to the high mobility of grain-boundary dislocations, stress concentrations created by dislocation pile-ups on grain boundaries can be relaxed plastically through an emission of lattice dislocations. This is accompanied by slip propagation across the grain boundaries coupled with the generation and motion of grain-boundary dislocations. A reduction of stress concentration at grain-boundary regions diminishes the tendency towards brittle intercrystalline fracture. This hypothesis was found to be consistent with studies of grain-boundary structure and grain-boundary dislocation geometry in Ni_3Al alloy with boron [26] and without boron [32], and was confirmed by results of mechanical tests [28, 29, 33].

The objective of the present work was to examine the influence of cold deformation (cold working) and annealing on yield strength, ultimate tensile strength, elongation and fracture behaviour of a polycrystalline Ni_3Al alloy containing zirconium and boron. The fracture behaviour of the polycrystalline alloy is discussed in terms of degree of cold deformation, annealing and strain rate.

2. Material and experimental procedure

The material used in this investigation was polycrystalline Ni_3Al containing zirconium and boron. The chemical composition of the alloy is listed in Table I. Zirconium additions aid improvement of high-temperature strength through solid solution hardening effects, while microalloying with boron enhances grain-boundary cohesive strength and helps improve ductility at ambient temperature [33–35]. The nickel aluminide, Ni_3Al, intermetallic compound has an $L1_2$ ordered crystal structure in the solid state. The unit cell has an ordered f c c lattice structure with nickel atoms occupying the face-centred sites and the aluminium atoms occupying corner sites, so that each aluminium atom has only nickel atoms for nearest neighbours. The flat tensile samples used were punched out of longitudinal sheets of the polycrystalline material that were cold rolled to different degrees of reduction ranging from 11.4 %–61.4 %. A few of the samples taken from each cold-rolled sheet were annealed in a controlled environment at 1100 °C for 1 h. A schematic drawing of the test specimen is shown in Fig. 1. Related parameters are given in Table II.

Metallographic samples were cut from the as-received test samples, mounted in bakelite, and wet ground on 320, 400 and 600 grit silicon carbide (SiC) paper using water as lubricant and then mechanically polished with 1 and 0.05 μm alumina-based polishing compound. Grain morphology was revealed using an etch comprising of a mixture of 20 H_2O, 20 HNO_3, 10 HF, 20 H_3PO_4, 10 acetic acid and 10 HCl (parts by volume). The specimens were etched for 180 s and examined by optical microscopy and photographed using standard bright-field techniques.

The tensile tests were carried out in controlled laboratory air environment (relative humidity 55 %) and at ambient temperature (23 °C). The tests were performed using a computer-controlled servohydraulic Instron test machine at nominal strain rates of 10^{-5} and 10^{-3} s^{-1}. The surfaces of the tensile samples were ground with 600 grit silicon carbide paper and then mechanically polished to remove all scratches. The yield stresses were measured at 0.2 % plastic strain, and ductility of the tensile test samples were evaluated from total elongation to failure, that is, the total strain to fracture or failure.

TABLE I Nominal chemical composition (wt %) of the nickel aluminide

Al	B	Cr	Fe	Mn	Mo	P	Zr	Si	Ní
11.12	0.044	0.046	0.450	0.024	0.002	0.002	0.78	0.03	Bal.

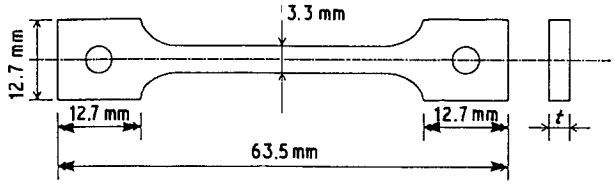

Figure 1 Schematic drawing showing configuration of tensile test specimen. See also Table II.

TABLE II

Condition	Nominal thickness, t (mm)
Undeformed sheet	1.1176
11.4 % CR[a]	0.9906
20.4 % CR	0.889
27.3 % CR	0.8128
36.4 % CR	0.7112
43.2 % CR	0.6350
47.7 % CR	0.5842
54.5 % CR	0.508
58.1 % CR	0.4572
64.1 % CR	0.4312

[a] Cold rolled.

Fracture surfaces of the deformed tensile samples were examined in a scanning electron microscope (SEM) to determine the predominant fracture mode and to characterize the fine-scale fracture features on the surface.

3. Results and discussion

3.1. Microstructure

The optical microstructure of the cold-deformed material is shown in Fig. 2 and compared with the microstructure of the undeformed material. Increasing the cold deformation on the polycrystalline alloy resulted in a refined or small grain size. The microstructure of the annealed samples is shown in Fig. 3. Annealing resulted in a recrystallized microstructure with fairly well-defined grain boundaries. The grain size of the polycrystalline alloy progressively decreased with increasing amount of cold deformation from 0 % (undeformed material) to 61.4 %.

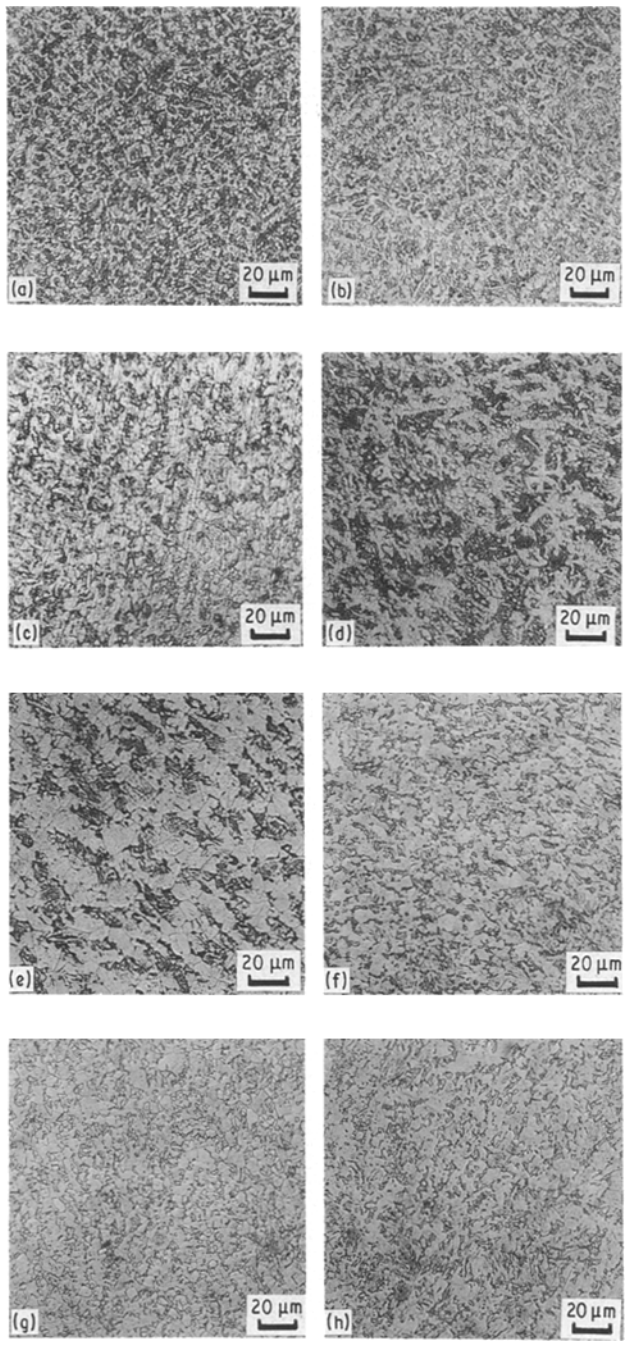

Figure 2 Optical micrographs showing microstructures of the undeformed and cold rolled (CR) polycrystalline $Ni_3Al + B$ intermetallic alloy: (a) undeformed, (b) 11.4% CR, (c) 27.3% CR, (d) 36.4% CR, (e) 47.7% CR, (f) 54.5% CR, (g) 59.1% CR, (h) 61.4% CR.

3.2. Tensile properties

3.2.1. Effect of cold deformation

A compilation of the monotonic mechanical properties of the polycrystalline alloy ($Ni_3Al + Zr + B$) cold deformed (cold worked) to various levels, tested at the two strain rates (10^{-5} and $10^{-3}\ s^{-1}$), are given in Tables III and IV. Duplicate samples were tested for each condition and no significant variation between the pairs of samples was observed.

3.2.1.1. Strain rate of $10^{-5}\ s^{-1}$

(a) At the strain rate of $10^{-5}\ s^{-1}$ the 0.2 % offset yield strength increased with an increase in cold deformation given to the undeformed sheet material. The maximum attainable yield strength (1473 MPa at 58.1 % cold deformation) is nearly three times the corresponding value for the undeformed sheet (458 MPa).

(b) The ultimate tensile strength follows the same trend as the yield strength. The maximum tensile strength (1901 MPa) is attained for the 58.1 % cold-deformed material and is twice the value of the undeformed sheet material (856 MPa).

(c) Fracture occurred at the maximum load and the fracture stress is equal to the ultimate tensile strength of the material.

(d) The total elongation to failure (ductility) decreased with an increase in strength. The elongation of the undeformed sheet material $Ni_3Al + Zr + B$ alloy (26.4 %) is three times the elongation achieved for

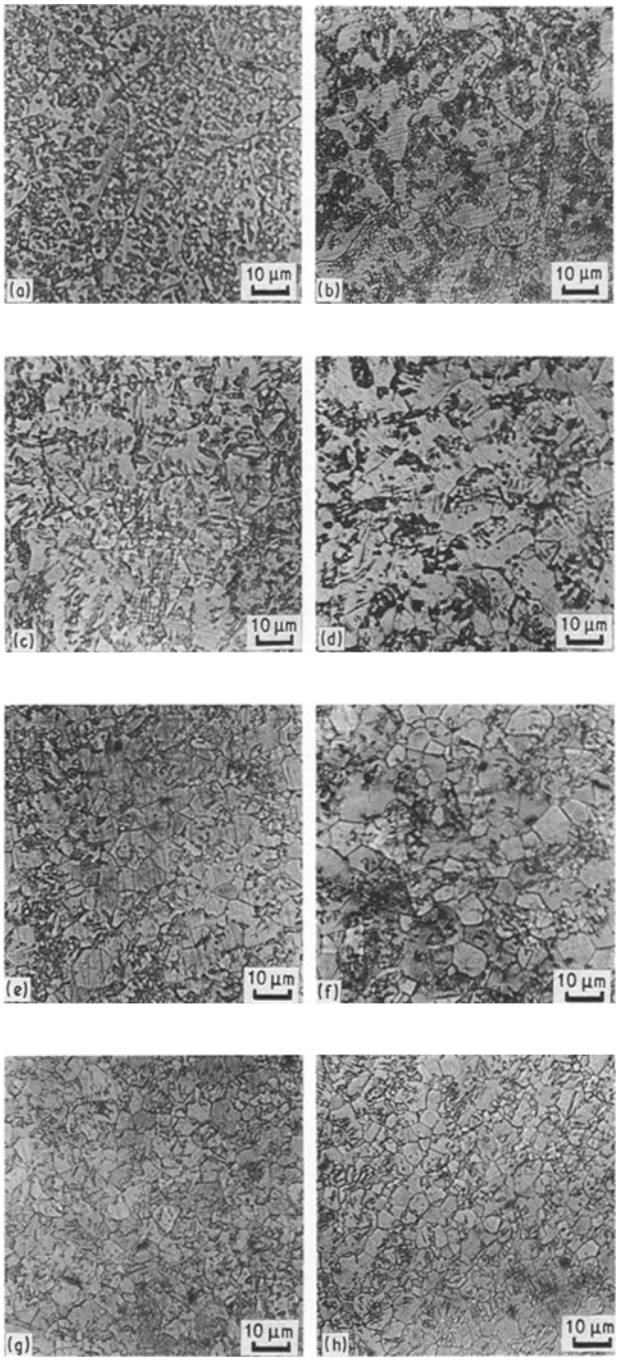

Figure 3 Optical micrographs of the cold rolled (CR) plus annealed polycrystalline $Ni_3Al + B$ intermetallic alloy: (a) undeformed, (b) 11.4%, (c) 27.3%, (d) 36.4%, (e) 47.7%, (f) 54.5%, (g) 59.1%, (h) 61.4%.

the material in the maximum strength condition (UTS = 1901 MPa, 58.1 % cold deformation). The variation of yield strength and ultimate tensile strength with per cent cold deformation is illustrated in Fig. 4.

3.2.1.2. Strain rate = 10^{-3} s^{-1}

(a) The variation of yield stress and ultimate tensile strength, with degree of cold deformation, at the higher strain rate of 10^{-3} (Table IV) follows a similar trend as at the lower strain rate (10^{-5} s^{-1}, Table III). This variation in strength is shown in Fig. 5, and reveals a progressive increase in both yield strength and ultimate tensile strength with increasing cold deformation.

(b) At this strain rate (10^{-3} s^{-1}) the elongation to failure of the undeformed material (35.2 %) is over five times greater than the corresponding value (6.4 %) for the material in the maximum strength condition (58.1 % cold deformed), and six times the corresponding value (5.6 %) for the sheet material given maximum cold deformation (61.4 %).

The observed increase in both yield strength and ultimate tensile strength, at the two strain rates, is attributed to intrinsic effects of strain-hardening arising from an increased dislocation density in the matrix due to the extrinsic influence of cold deformation on the polycrystalline $Ni_3Al + B$ intermetallic.

A comparison of the elongation to failure for the different conditions, at the two strain rates, is made in Fig. 6. It is observed from this figure that strain rate has only a marginal influence on elongation to failure. The elongations at the two strain rates vary within 10 % of each other and exhibit the same general trend with an increase in amount of cold deformation imparted to the polycrystalline alloy.

3.2.2. Effect of annealing

The cold deformed tensile samples were annealed for 1 h at 1100 °C prior to tensile testing. A compilation of the monotonic mechanical properties of the cold-deformed plus annealed samples, at strain rates of

TABLE III Monotonic mechanical properties of the polycrystalline $Ni_3Al + Zr + B$ alloy in the cold-deformed condition at strain rate of 10^{-5} s^{-1}. Results are mean based on two tests.

Condition	Yield stress (Mpa)	Ultimate tensile stress (MPa)	Elongation (%)	Fracture stress (MPa)
Undeformed sheet	458	856	26.4	856
11.4 % CR	707	993	20.8	993
20.4 % CR	1000	1341	13.6	1341
27.4 % CR	1127	1442	12.0	1442
36.4 % CR	1257	1610	11.2	1610
43.2 % CR	1323	1676	8.8	1676
47.7 % CR	1360	1764	8.8	1764
54.5 % CR	1419	1817	8.0	1817
58.1 % CR	1473	1901	8.0	1901
61.4 % CR	1373	1872	6.4	1872

TABLE IV Monotonic mechanical properties of the polycrystalline $Ni_3Al + Zr + B$ alloy in the cold-deformed condition at strain rate of $10^{-3}\ s^{-1}$. Results are mean based on two tests.

Condition	Yield stress (Mpa)	Ultimate tensile stress (MPa)	Elongation (%)	Fracture stress (MPa)
Undeformed sheet	433	916	35.2	916
11.4% CR	707	1149	26.4	1149
20.4% CR	1061	1374	12.0	1374
27.4% CR	1146	1483	10.4	1483
36.4% CR	1288	1648	11.2	1648
43.2% CR	1358	1665	10.4	1665
47.7% CR	1406	1718	8.8	1718
54.5% CR	1480	1817	8.0	1817
58.1% CR	1591	1901	6.4	1901
61.4% CR	1342	1700	5.6	1700

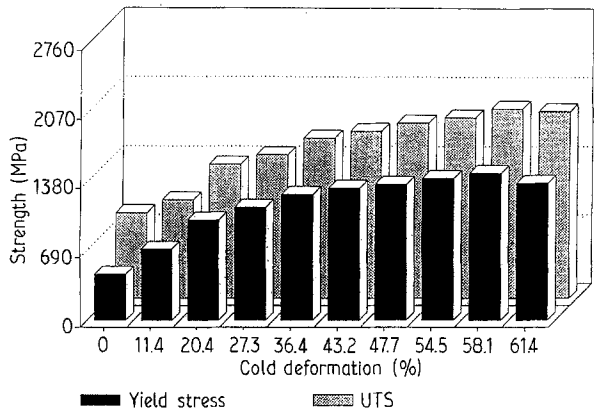

Figure 4 Variation of yield strength and ultimate tensile strength with degree of cold deformation, at a strain rate of $10^{-5}\ s^{-1}$ in laboratory air.

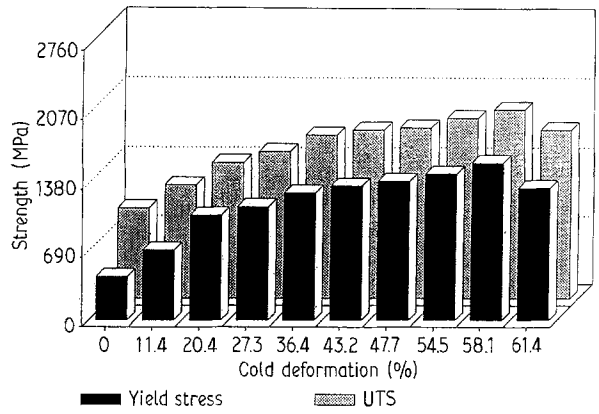

Figure 5 Variation of yield strength and ultimate tensile strength with degree of cold deformation, at a strain rate of $10^{-3}\ s^{-1}$ in laboratory air.

10^{-5} and $10^{-3}\ s^{-1}$, is given in Tables V and VI. The salient observations are given below.

3.2.2.1. Strain rate = $10^{-5}\ s^{-1}$

(a) The yield stress and ultimate tensile stress increased with an increase in cold deformation up to 54.5%. The maximum strength (YS: 1061 MPa, UTS: 1850 MPa) is attained for the material that is cold deformed 54.5 %. While annealing at 1100 °C relieves the effects of strain hardening arising from an increased dislocation density due to cold deformation, the increase in strength is attributed to an overall refinement in the grain structure (Fig. 3) of the Ni_3Al intermetallic compound with an increase in cold deformation given to the undeformed polycrystalline material. The variation of strength for the different conditions is illustrated in Fig. 7.

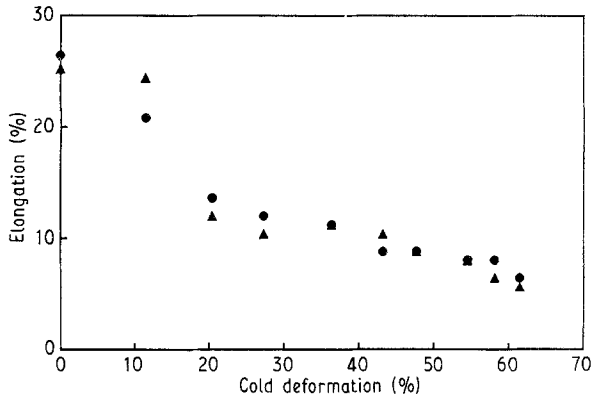

Figure 6 Effect of cold deformation on elongation to failure at a strain rate of (●) $10^{-5}\ s^{-1}$, and (▲) $10^{-3}\ s^{-1}$ in laboratory air.

(b) Fracture of the cold-deformed plus annealed samples occurred at the maximum load, and the variation of fracture stress is the same as that of the ultimate tensile stress.

(c) The elongation to failure showed no observable trend for the fully annealed samples. The variation of elongation to failure for the different conditions was random and well within 10 % of each other.

3.2.2.2. Strain rate = $10^{-3}\ s^{-1}$. The key observations at the higher strain rate were as follows.

(a) The yield stress and ultimate tensile stress were found to increase with cold deformation. The maximum strengths (YS: 544 MPa, UTS: 1278 MPa) were attained for the material that was cold deformed 58.1 %. The variation in strength for the different conditions is shown in Fig. 8.

(b) The variation of fracture stress was similar to the ultimate tensile stress, because, for all conditions, fracture occurred at the maximum load.

(c) The elongation to failure revealed no observable trend and the variations in elongation for the different

TABLE V Monotonic mechanical properties of the polycrystalline Ni_3Al alloy in laboratory air at a strain rate of $10^{-5}\ s^{-1}$. Results are mean based on two tests.

Condition	Yield stress (Mpa)	Ultimate tensile stress (MPa)	Elongation (%)	Fracture stress (MPa)
Undeformed sheet	362	1019	30.4	1019
11.4 % CR	408	1149	33.5	1149
20.4 % CR	424	1144	33.2	1144
27.4 % CR	481	1243	31.2	1243
36.4 % CR	493	1203	31.2	1203
43.2 % CR	615	1258	28.8	1258
47.7 % CR	668	1222	32.8	1222
54.5 % CR	1061	1850	32.8	1850
58.1 % CR	639	1420	32.8	1420
61.4 % CR	562	1295	32.8	1295

TABLE VI Monotonic mechanical properties of the polycrystalline $Ni_3Al + Zr + B$ alloy in the cold-deformed plus fully annealed condition at strain rate of $10^{-3}\ s^{-1}$. Results are mean based on two tests.

Condition	Yield stress (Mpa)	Ultimate tensile stress (MPa)	Elongation (%)	Fracture stress (MPa)
Undeformed sheet	307	927	26.4	927
11.4 % CR	411	1126	36.9	1126
20.4 % CR	479	1167	32.4	1167
27.4 % CR	486	1227	30.9	1227
36.4 % CR	481	1172	31.9	1172
43.2 % CR	507	1203	33.4	1203
47.7 % CR	541	1223	32.6	1223
54.5 % CR	515	1176	31.2	1176
58.1 % CR	544	1278	30.5	1278
61.4 % CR	536	1224	36.3	1224

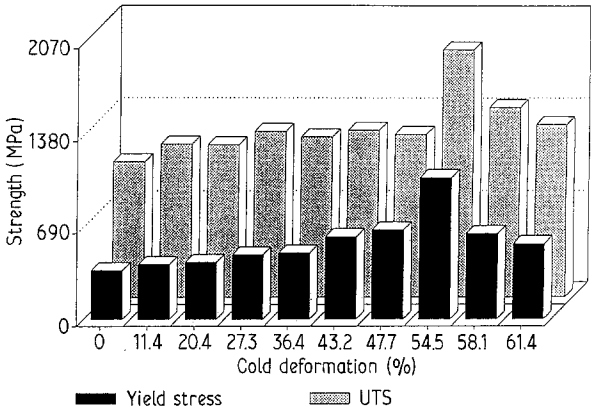

Figure 7 Variation of yield stress and ultimate tensile stress for the cold-deformed plus annealed test samples deformed at a strain rate of $10^{-5}\ s^{-1}$ in laboratory air.

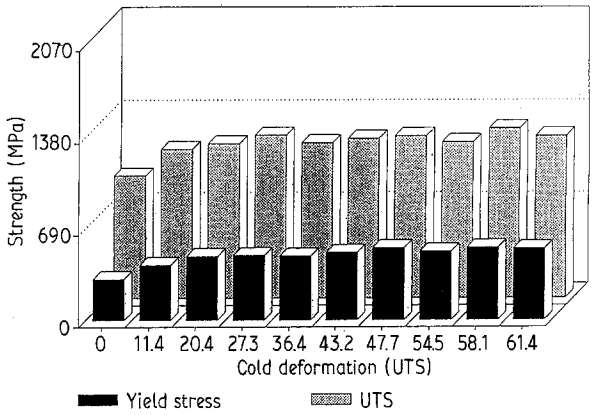

Figure 8 Effect of cold deformation on yield strength and ultimate tensile strength of the cold-deformed plus annealed samples deformed at strain rate of $10^{-3}\ s^{-1}$ in laboratory air.

conditions were well within 10 %–15 %. This pattern is quite similar to the trend observed at the lower strain rate ($10^{-5}\ s^{-1}$).

A comparison of elongations to failure of the cold-deformed and the cold-deformed plus annealed samples, at the two strain rates, is made in Fig. 9. This figure reveals an approximate two-fold improvement in elongation to failure (tensile ductility) resulting from fully annealing the cold-deformed samples. The influence of annealing on tensile behaviour of the polycrystalline $Ni_3Al + Zr + B$ alloy is best represented by a comparison of the engineering stress–engineering strain curves of the cold-deformed and cold-deformed plus annealed samples (Fig. 10). Annealing the cold-deformed samples resulted in a degradation in strength but with a substantial improvement in strain to failure or elongation. It seems plausible that annealing, at 1100 °C, causes two independent phenomenon to occur:

(i) relief of the intrinsic effects of strain hardening resulting from cold working the material; and

(ii) promotion of a recrystallized microstructure (Fig. 3).

A reduction or elimination of strain-hardening effects results in degradation in strength with a resultant improvement in ductility.

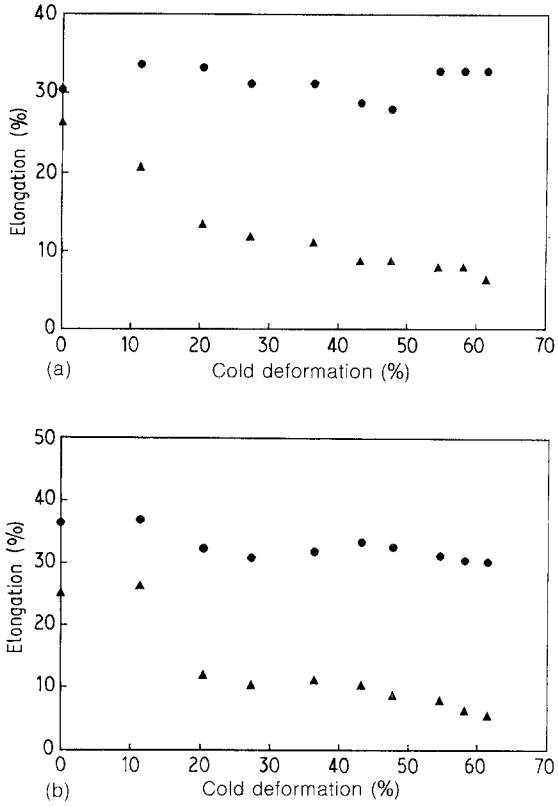

Figure 9 Effect of annealing on elongation to failure of the cold-deformed tensile samples. (a) $10^{-5}\,s^{-1}$, (b) $10^{-3}\,s^{-1}$. (●) With anneal, (▲) without anneal.

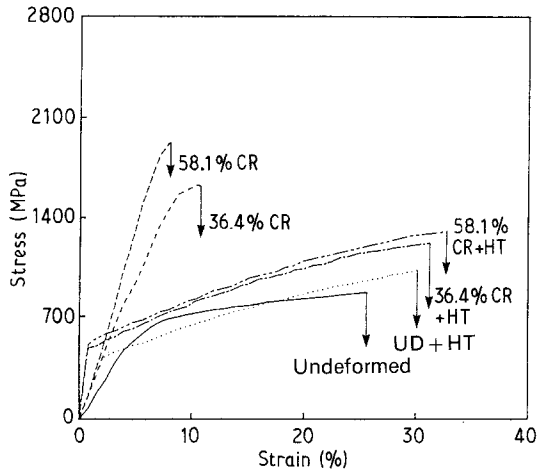

Figure 10 Comparison of the influence of annealing the cold-deformed samples on engineering stress–strain curves of the polycrystalline intermetallic compound. UD, undeformed; HT, heat treated; CR, cold rolled.

3.3. Fracture behaviour

The monotonic fracture surfaces are helpful in elucidating microstructural effects on ductility and fracture properties of the polycrystalline $Ni_3Al + Zr + B$ intermetallic alloy. Examination of the fracture surface features in a scanning electron microscope, of the deformed tensile specimens was done at low magnification to identify the overall fracture morphology, and at higher magnification to identify the fine-scale fracture surface features. Samples for SEM observation were obtained from the deformed tensile specimens by sectioning parallel to the fracture surface. Fractography of the tensile samples revealed different features for the as-cast and cold-deformed specimens. Representative fracture features of both the non-heat-treated and heat-treated (annealed) samples deformed to failure at the two strain rates are shown in Figs 11–14.

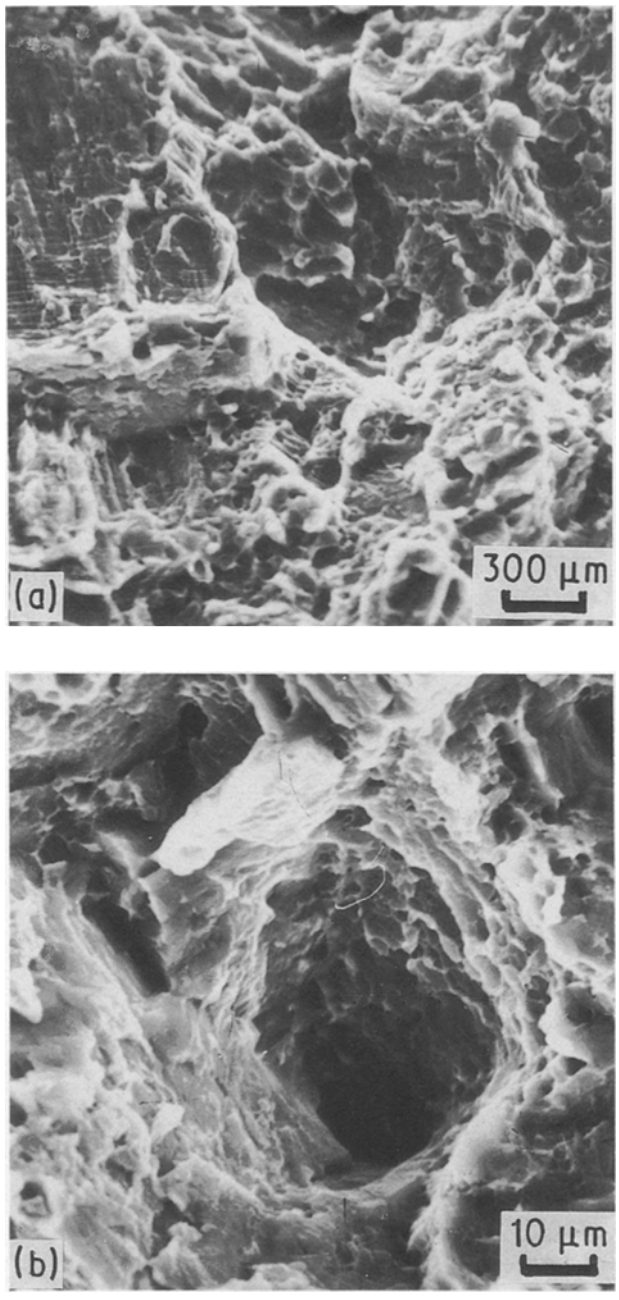

Figure 11 Scanning electron micrographs showing fracture surface features of the material in the undeformed condition: (a) voids on fracture surface, (b) macroscopic void surrounded by dimples.

On a macroscopic scale the following features were seen.

(a) Tensile fracture of the undeformed material was transgranular. Examination of the fracture surface at higher magnifications revealed a population of microvoids, of a wide range of sizes, distributed randomly across the fracture surface (Fig. 11a). Few macroscopic voids (Fig. 11b) were found intermingled with the microscopic voids, indicating ductile failure. Shallow dimples were found on the transgranular fracture regions in areas between voids and surrounding the macrovoids.

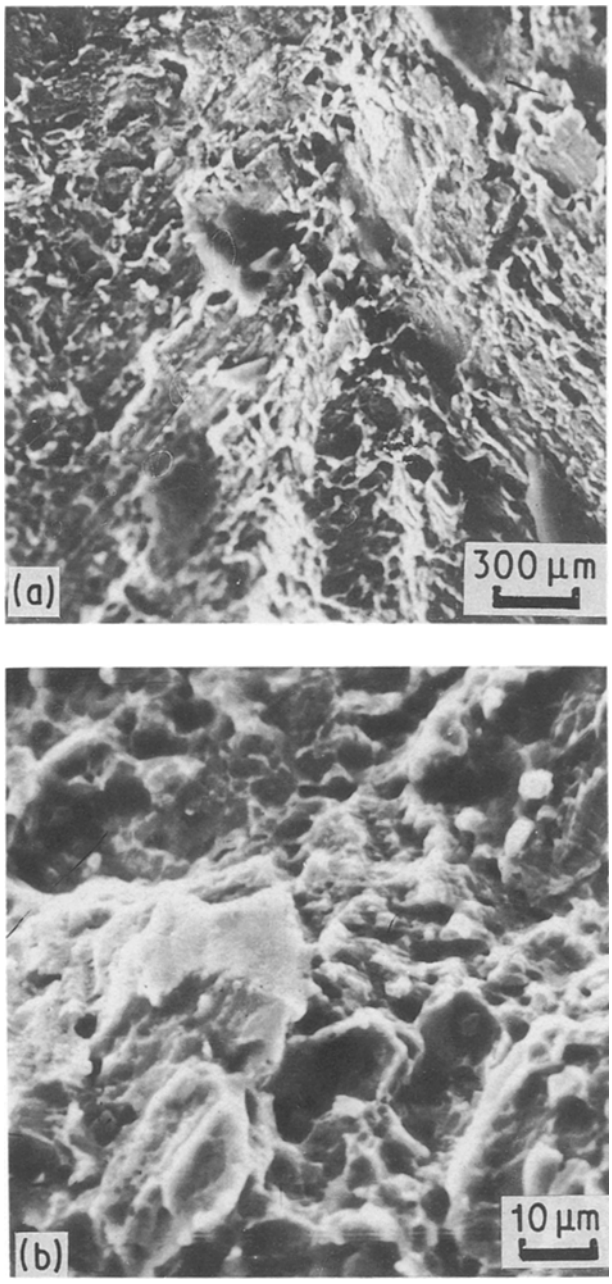

Figure 12 Scanning electron micrograph showing fracture surface features of the undeformed plus annealed samples: (a) transgranular fracture, (b) voids on the transgranular fracture surface.

(b) Fracture of the undeformed plus annealed samples was also transgranular (Fig. 12a). Examination of the tensile fracture surface at higher magnification revealed fine microscopic voids randomly distributed across the fracture surface (Fig. 12b). The area between voids was covered with shallow dimples.

(c) Tensile fracture of the samples subjected to maximum cold deformation (61.4 %) was predominantly transgranular at both strain rates (Fig. 13). Examination at higher magnification revealed the transgranular fracture regions covered with shallow dimples (Fig. 13b). Small second-phase particles were found associated with the shallow dimples (Fig. 13c).

(d) Fracture morphology of the samples that were cold deformed 61.4 % and then annealed were quite different from the cold-deformed and non-heat-treated counterpart. Fracture was bimodal with evidence of

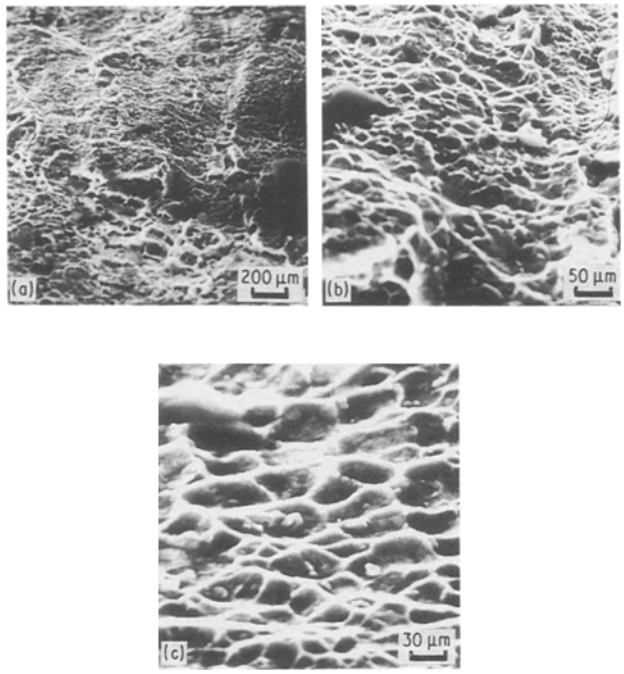

Figure 13 Scanning electron micrograph of the 61.4% CR sample showing: (a) predominantly transgranular fracture, (b) shallow dimples on transgranular surface, and (c) small second-phase particles distributed at random within the shallow dimples.

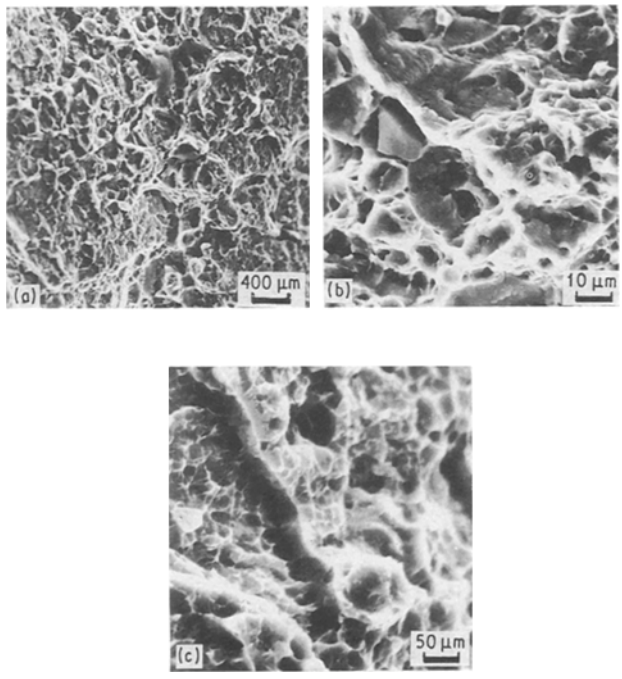

Figure 14 Scanning electron micrographs showing fracture surface features of samples cold deformed 68.1 % and then annealed: (a) evidence of intergranular cracking, (b) macroscopic and microscopic voids, (c) shallow near-equiaxed dimples.

traces of intergranular cracking (Fig. 14a). Examination of the fracture surface at higher magnification revealed macroscopic voids intermingled with numerous microscopic voids, indicating ductile rupture (Fig. 14b). Shallow near-equiaxed dimples were found adjacent to the intergranular fracture regions (Fig. 14c). During tensile deformation the progressive build-up of dislocations at grain boundaries results in

stress concentration. The localization of stresses facilitates nucleation of voids at the inclusions and impurities along the grain boundaries. The fine microvoids coalesce and the halves of these voids are the dimples visible on the fracture surface.

4. Conclusions

Based on a study of the influence of cold deformation and annealing on the room-temperature tensile behaviour of polycrystalline Ni_3Al alloy containing zirconium and boron, tested at two strain rates, the following are the main conclusions.

1. Annealing the cold-deformed material resulted in a recrystallized microstructure. Increasing the amount of cold deformation resulted in a material having refined microstructure, that is smaller grain size.

2. Strength of the polycrystalline alloy increased with an increase in cold deformation. The increase in strength was marked by a degradation in elongation to failure (ductility). The degradation in ductility was as high as 300%.

3. Annealing the cold-deformed samples was observed to degrade both yield strength and ultimate tensile strength.

4. The annealed samples exhibited improved ductility (elongation to failure) over the cold-deformed counterpart. The improvement in ductility or elongation to failure was appreciable with increasing amount of cold deformation given to the undeformed polycrystalline intermetallic material.

5. Strain rate was found to have only a little influence on strength and elongation to failure of both cold deformed and fully annealed material.

6. Tensile fracture of the polycrystalline intermetallic in the undeformed condition and the undeformed plus annealed condition was predominantly transgranular with macroscopic and microscopic voids dispersed on the fracture surface.

7. For the cold-deformed conditions, fracture of the tensile samples was predominantly transgranular with shallow dimples on the transgranular fracture surface. For the cold-deformed and fully annealed material, fracture surfaces comprised of a population of voids, of a wide range of sizes.

Acknowledgements

The present study was partially supported by the Ohio board of Regents under Grant No. 5-34021. Material used in this study was provided by Oak Ridge National Laboratory, Oak Ridge, Tennessee. Thanks are due to Dr Vinod K. Sikka, Program Manager, for his encouragement and help in procuring the material, and Mr Todd Hoff for providing experimental assistance during the experimental phase of this study.

References

1. M. H. YOO, J. A. HORTON and C. T. LIU, *Acta Metall.* **36**(11) (1988) 2935.
2. P. A. FLINN, *Trans TMS-AIME* **218** (1960) 145.
3. R. G. DAVIS and N. S. STOLOFF, *ibid.* **233** (1965) 714.
4. E. A. AITKEN, "Intermetallic Composites" (Wiley Interscience, New York, 1967) pp. 491–550.
5. E. M. GRALA, "Mechanical Properties of Intermetallic Compounds", edited by J. H. Westbrook (Wiley, New York, 1960), p. 358.
6. K. AOKI and O. IZUMI, *Nippon Kinzoku Gokkaishi* **41** (1977) 170.
7. R. MOSKOVICH, *J. Mater. Sci.* **13** (1978) 1901.
8. A. V. SEYBOLT and J. H. WESTBROOK, *Acta Metall.* **12** (1967) 449.
9. K. AOKI and O. IZUMI, *Trans. Jpn Inst. Metals* **19** (1978) 203.
10. G. W. GROVES and A. KELLY, *Phil. Mag.* **8** (1963) 877.
11. C. T. LIU and J. O. STIEGLER, *Science* **226** (1984) 636.
12. S. V. RAJ, R. D. NOEBE and R. BOWMAN, *Scripta Metall.* **23** (1989) 2049.
13. C. T. LIU, C. L. WHITE and J. A. HORTON, *Acta Metall.* **33** (1985) 213.
14. C. T. LIU and C. L. WHITE, *ibid.* **35** (1987) 643.
15. C. T. LIU, *Mater. Res. Soc. Symp. Proc.* **81** (1987) 355.
16. P. S. KHADKIKAR, J. J. LEWANDOWSKI and K. VEDULA, *Metall. Trans.* **20A** (1989) 1247.
17. J. J. LEWANDOWSKI, G. MICHAL, I. LOCCI and J. J. RIGNEY, *Mater. Res. Soc. Symp. Proc.* **84** (1990).
18. K. AOKI and O. IZUMI, *Nippon Kinzaku Gakkaishi* **43** (1979) 1190.
19. A. I. TAUB, S. C. HUANG and K. M. CHANG, *Metall. Trans.* **15A** (1984) 399.
20. *Idem, Mater. Res. Soc. Symp. Proc.* **39** 1985, p. 221.
21. A. I. TAUB, K. M. CHANG and C. T. LIU, *Scripta Metall.* **20** (1986) 1613.
22. I. BAKER, E. M. SCHULSON and J. A. HORTON, *Acta Metall.* **35** (1987) 1533.
23. C. L. WHITE, R. A. PADGETT, C. T. LIU and S. M. YALISOVE, *Scripta Metall.* **18** (1984) 1417.
24. A. CHOUDHURY, C. L. WHITE and C. R. BROOKS, *ibid.* **20** (1986) 1061.
25. J. J. LEWANDOWSKI, C. A. HIPPSLEY, M. B. D. ELLIS and J. F. KNOTT, *Acta Metall.* **35** (1987) 593.
26. M. S. KIM, S. HANADA, S. WATANABE and O. IZUMI, *J. Mater. Sci.* **25** (1990) 1590.
27. C. L. WHITE, R. A. PADGETT, C. T. LIU and S. M. YALISOVE, *Scripta Metall.* **18** (1984) 1417.
28. E. M. SCHULSON, T. P. WEIHS, J. BAKER, H. J. FROST and J. A. HORTON, *Acta Metall.* **34** (1986) 1395.
29. T. P. WEIHS, V. ZINOVIEV, D. V. VIENS and E. M. SCHULSON, *ibid.* **35** (1987) 1109.
30. C. L. BRIANT and R. P. MESSMER, *Phil. Mag.* **12** (1980) 568.
31. R. P. MESSMER and C. L. BRIANT, *Acta Metall.* **30** (1982) 457.
32. J. A. HORTON and M. K. MILLER, *ibid.* **33** (1987) 133.
33. E. M. SCHULSON, T. P. WEIHS, D. V. VIENS and J. BAKER, *ibid.* **33** (1985) 1587.
34. C. T. LIU and V. K. SIKKA, *J. Metals* **38** (5) (1986) 19.
35. R. N. WRIGHT and V. K. SIKKA, *J. Mater. Sci.* **23** (1988) 4315.

Received 18 September 1991
and accepted 7 January 1992